APPENDIX

A. PHOTON CONVERSIONS

The probability η that a photon generated in the interaction region converts in matter before reaching hodoscope H1 affects the background level for the form factor events (Section 3.4).

I measure this probability using data from a special total-energy trigger without hodoscope vetoes. This trigger simply requires that the energy deposited in the CCAL be at least 80% of the total energy in the lab frame; it is referred to as ETOT 80% no-veto.

From this sample, a clean $\pi^0\pi^0 \to 4\gamma$ subset is selected, by requiring exactly four clusters in the CCAL with their centers between ring 2 and ring 18 included. For the 5439 events that survive, the four clusters are paired according to which combination gives the best $\pi^0\pi^0$ kinematics, quantified by the minimum value of the variable:

$$(w_\theta \cdot \Delta\theta)^2 + (w_\phi \cdot \Delta\phi)^2 . \tag{A.1}$$

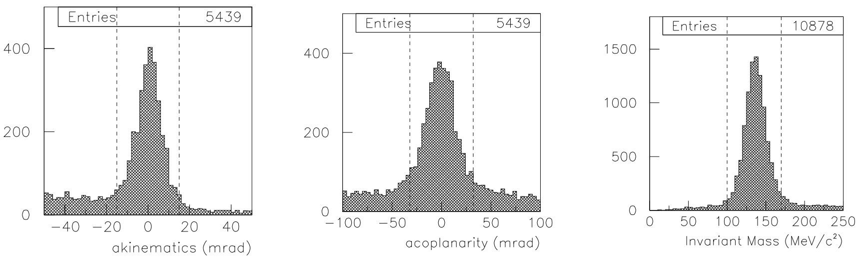

Fig. A.1: Distribution of akinematics, acoplanarity and candidate pion mass for four-cluster events from the total-energy study trigger.

The akinematics $\Delta\theta$ is defined as the difference between two quantities: (a) the value of the forward pion's polar angle predicted from the backward pion according to two-body kinematics and (b) the measured value of the forward pion's polar angle. $\Delta\phi$ is the acoplanarity, ie $|\phi_1 - \phi_2| - \pi$, which measures the azimuthal deviation from two-body kinematics. The weight w_θ is twice as large as the weight w_ϕ; it is determined a posteriori from the widths of the akinematics and acoplanarity distributions (Figure A.1). After the four clusters have been paired, three cuts are applied:

- invariant mass of the both candidate photon pairs within a ± 35 MeV window centered around the π^0 rest energy (=135 MeV);
- absolute value of the akinematics smaller than 15 mrad;
- absolute value of the acoplanarity smaller than 32 mrad.

The corresponding distributions before these three cuts are shown in Figure A.1. The final clean sample contains 2585 events, or 10340 tracks.

If one of the four calorimeter clusters is associated with a coincidence between hodoscopes H1 and H2$'$ (or H2), then it is identified as a photon conversion or as a Dalitz decay of the pion.

The opening angle of the photons coming from the same pion is small compared to the hodoscope granularity. Often ($\simeq$ 75% of the times), if one of the two photons is associable with a hodoscope line, the other one is too. Neglecting this fact would make most of the conversions count as two, and this would end up in an overestimation of the conversion probability η. To avoid this, I make the assumptions that the conversion probabilities of the two photons are independent and that η^2 or $\eta \cdot \delta$ (δ = 0.6% is the Dalitz probability per cluster) are small compared to η. Each time both clusters are associated with a hodoscope coincidence, the event is registered as a single occurence of a conversion or a Dalitz decay.

The results are shown in Figure A.2 as a function of the polar and azimuthal angles. Since Dalitz decays cannot be distinguished from conversions, the fraction of CCAL clusters with an associated charged track is the sum of two independent contributions. The Dalitz contribution per cluster is 0.6%. What is left (less than 1.7%), is attributed to photon conversions[a]; it is consistent with estimates that employ the thickness of the material between the interaction region and hodoscope H1. This value η = 1.7% is used in Section 3.4 to evaluate the form factor background due to neutral pions and photons.

[a] I am neglecting the detection inefficiency of the hodoscopes, H1 in particular.

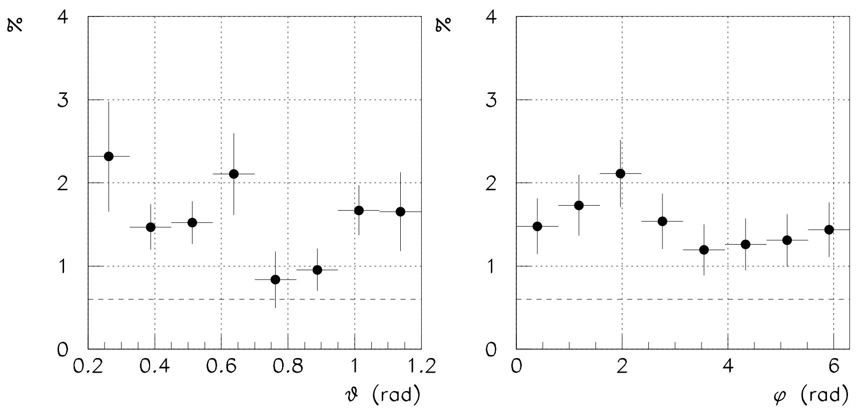

Fig. A.2: Probability of photon conversions or Dalitz decays before H1, as a function of the polar and azimuthal angles. The horizontal dashed line represents the contribution attributed to Dalitz decay.

B. PION REJECTION

The reaction $\bar{p}p \rightarrow \pi^+\pi^-$ contributes to the background for the form-factor selection (Section 3.4). I selected a sample of $\pi^+\pi^-$ events to measure the pion rejection inefficiency of the Čerenkov counter and of the CCAL. Both detectors contribute to the rejection of the first-level trigger and of the Electron-Weight algorithm. The main cause of inefficiency in the Čerenkov counter is the emission of δ-rays by a charged track. In the CCAL, the discrimination between hadrons and electrons or positrons is based on the magnitude and on the shape of the energy deposition.

Since the E-835 detector has not been designed to select hadrons (and much less to identify them), the $\pi^+\pi^-$ sample cannot be as clean as the e^+e^- samples are. Still, there are two trigger types which can be suitable for selecting the charged pion sample:

- minimum-bias trigger, requiring just two hits in the calorimeter above 100 MeV; these events have been collected at low rate throughout the data-taking run, with a prescaling factor of 10^5;

- two-body hadronic trigger, taken only once ($\sqrt{s} = 2.951$ GeV, runs 2225–2230, $L = 605\ \text{nb}^{-1}$, prescaling factor of 1.2×10^2), and used to measure the efficiency of the proton-antiproton trigger. This logic is defined as $(2h) \cdot (\text{H2} = 2) \cdot (\text{COPL}) \cdot (\overline{\text{FCH}})$; the symbols are explained in Section 3.1.(b).

There is also a limited set of minimum-bias events taken with a lower

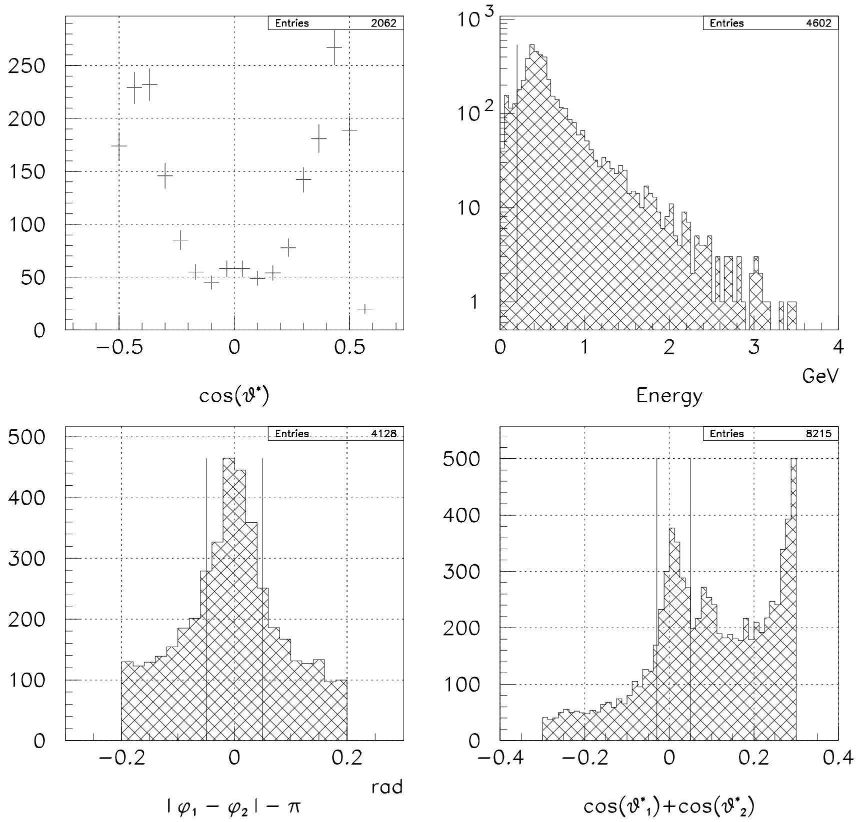

Fig. B.1: The $\pi^+\pi^-$ sample. The angular distribution of the tracks in the CM frame is shown on the top left (two entries per event). On the top right is the energy distribution before the energy cut (represented by the vertical line) and after all other cuts. The analogous plots for the acoplanarity and the $[\cos(\theta_1^*) + \cos(\theta_2^*)]$ distributions are shown at the bottom.

prescaling factor. For this study, I choose the $\bar{p}p$ study trigger, which is the most statistically significant.

Besides a strict two-cluster cut on the CCAL multiplicity, the off-line selection of $\bar{p}p \to \pi^+\pi^-$ is essentially based upon azimuthal and polar kinematics. The cuts are applied on cluster energy, acoplanarity $\equiv |\phi_1 - \phi_2| - \pi$ and on the sum $\cos(\theta_1^*) + \cos(\theta_2^*)$ of the cosines in the CM frame; the corresponding distributions are shown in Figure B.1, together with the cuts.

For each of the 2062 selected tracks, the probability of having a signal in the Čerenkov counter above 0.5 phe, which is the threshold used in the first-level trigger, is measured as a function of the polar and azimuthal angles (Figure B.2). The high rejection inefficiency in the upstream region is likely due to the phototube recesses; however, in the form factor analysis, that region is excluded from the fiducial volume. In the region between 15° and 60°, the average rejection inefficiency is 82/1646 = (5.0±0.5)%.

The fraction of tracks releasing in the CCAL an energy deposit compat-

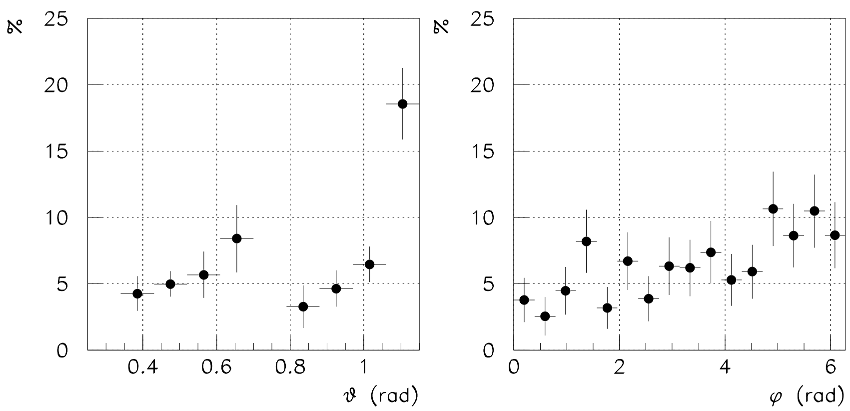

Fig. B.2: Pion rejection inefficiency of the Čerenkov counter as a function of the polar and azimuthal angles.

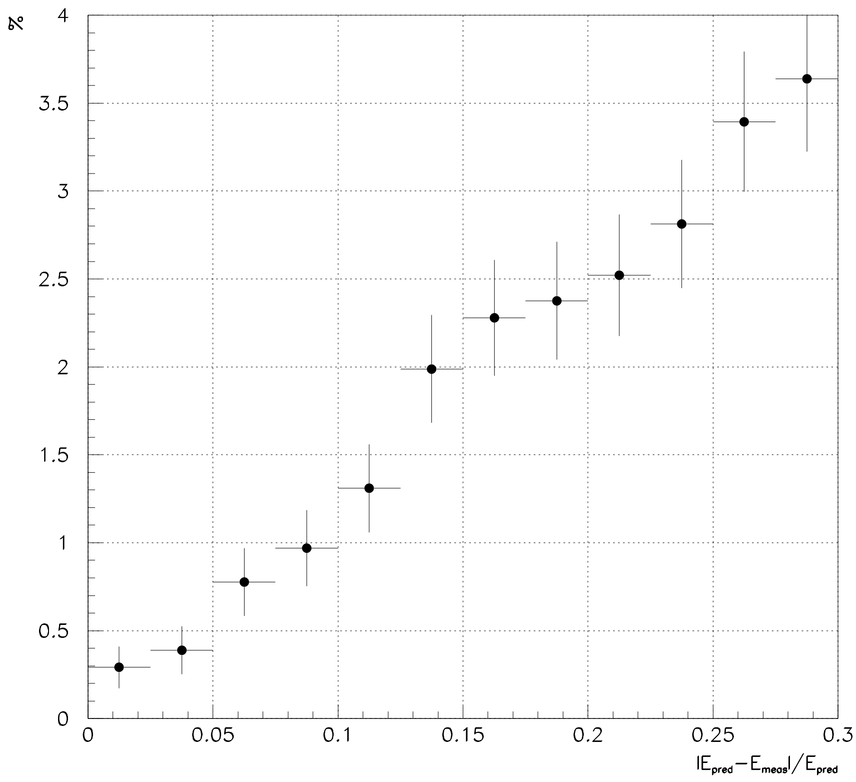

Fig. B.3: Fraction of pion showers having a measured energy compatible with an electron shower in the same polar region, as a function of the relative deviation from the predicted energy.

ible with the e^+e^- kinematics is also recorded. From Figure B.3, the probability of a pion shower of having an energy within 10% of the energy of an electron impinging in the same polar region is (1.0±0.2) %. This can be taken as the pion rejection inefficiency of the CCAL when the shape of the cluster is not used (for example, in the first-level trigger).

The sample is too small to evaluate the Čerenkov rejection at trigger level and at the EW level separately. For this reason, I also calculate an overall Čerenkov inefficiency, which includes the EW cut. An upper limit can be extracted by determining how often a pion track has $EW > 0$. In fact, the fraction of $\pi^+\pi^-$ events passing the EW cut used in the analysis ($\log_{10}(EW1 \cdot EW2) > 0$) will be a subset of those having both tracks with $EW > 0$. A clean sample of electron/positron tracks from the J/ψ is selected with kinematic cuts. The distribution of Čerenkov signal for the electron tracks with $EW > 0$ is plotted in Figure B.4. After normalization, this dis-

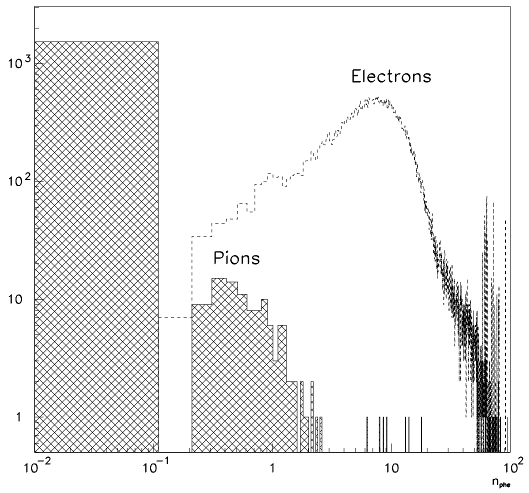

Fig. B.4: Distribution of Čerenkov signals for clean electron tracks and for events in the $\pi^+\pi^-$ sample.

tribution is interpreted as the derivative of the probability Π of passing the EW > 0 cut as a function of the number of photoelectrons n_{phe}. This is a conservative assumption, because it neglects the CCAL contribution to the EW. The probability Π is constrained to be zero at $n_{phe} = 0$ and approaches one as n_{phe} increases. The n_{phe} distribution for all pion tracks is also shown in Figure B.4. The probability κ of a pion track of passing the EW cut due to the Čerenkov signal is taken to be this distribution multiplied by Π and summed over n_{phe}. The result is $\kappa = (5{\pm}1){\times}10^{-3}$; I use this number in the background estimates of Section 3.4.